Graphene-β-Ga_2O_3 Heterojunction for Highly Sensitive Deep UV Photodetector Application

*Wei-Yu Kong, Guo-An Wu, Kui-Yuan Wang, Teng-Fei Zhang, Yi-Feng Zou, Dan-Dan Wang, and Lin-Bao Luo**

Photodetectors, as one of the most important optoelectronic devices, are capable of sensing electromagnetic irradiation, in most cases of optical power. They have attracted increasing research interest due to their wide-ranging applications in a number of areas such as emitter calibration, spatial optical communication, light vision, and biological and chemical sensors.[1] In comparison to the visible and infared light (IR) photodetectors, devices for detection of UV are of paramount importance and have recently received extensive attention for their promising application in military surveillance, target detection and acquisition, missile launch detection, and so on. To date, a number of low-dimensional wide bandgap semiconductors including ZnO, GaN, TiO_2, SnO_2, Ga_2O_3, etc. have been employed to fabricate a number of high-performance UV light photodetectors with various geometries.[2–4] Take Ga_2O_3 for example, various Ga_2O_3 nanostructures (e.g., nanowire,[5] nanobelt,[6–8] and nanosheet[9]) have been synthesized for photodetector applications. Despite this progress, the majority of the Ga_2O_3 nanostructure-based devices are still limited by relatively low quantum efficiency and responsivity, which is mainly attributed to the small photo-absorption cross section.[10]

In order to optimize the device performance of Ga_2O_3 based photodetectors, many groups have tried to assemble heterojunction device by combining Ga_2O_3 with other semiconductor materials such as GaN,[11] SnO_2,[12] and ZnO.[13] For instance, Zhao et al. reported avalanche photodetectors by growing a ZnO-Ga_2O_3 core–shell microwires. Thanks to the avalanche multiplication effect, the device demonstrated ultrahigh sensitivity and fast response speed.[13] Another solution to the above problem is to construct Schottky junction devices by combining nanostructure array or bulk semiconductor with graphene, which has been widely used to fabricate a number of high-performance optoelectronic device including, graphene/III-VI group semiconductors (GaN,[14] InP,[15] BN[16]), graphene/IV group semiconductors (Ge[17] and Si[18–20]), and graphene/II-VI group semiconductors (CdS[21] and ZnS[22]). Enlightened by the above study, we herein reported a simple deep UV photodetector (DUVPD) by coating multilayer graphene (MLG) on a beta-Ga_2O_3 substrate. It was found that the as-fabricated MLG-β-Ga_2O_3 heterojunction device exhibited obvious sensitivity to deep ultraviolet (DUV) light illumination (wavelength 254 nm) with good reproducibility and stability. It was also revealed that the photocurrent of the device was not only determined by the bias voltage but also by the light intensity. Further device analysis demonstrated that the MLG-β-Ga_2O_3 heterojunction device had very good spectral selectivity with peak sensitivity at around 220 nm. This result along with the easy fabrication process renders the present DUVPD promising building block for future optoelectronic system application.

The DUVPD is basically composed of single-crystalline Sn atoms doped *n*-type β-Ga_2O_3 wafer and chemical vapor deposition derived graphene (**Figure 1**a). The MLG-β-Ga_2O_3 heterojunction device with Ag on the MLG side and Cr/Au on the Ga_2O_3 side was mounted on a printed circuit board (PCB), as shown in Figure S1 (Supporting Information). For convenience, both the silver and Cr/Au electrodes were then connected to the PCB by 5 μm thick Al wires via wire bonding (Figure 1b). Field emission scanning electron microscopy (FESEM) image of the graphene film in Figure 1c reveals that the surface of graphene film is relatively smooth, with some wrinkles which were normally formed during graphene transfer at water.[16] Figure 1d illustrates an example of atomic force microscopy (AFM) image of the graphene film, on which a height profile was taken along the red curve. Apparently, the film has a thickness of 2 nm, corresponding to 3–5 layer of graphene.[23,24] From the Raman study of graphene shown in Figure 1e, one can see a weak D band and two strong bands due to the G and 2D band with ratio of I_{2D}/I_G of 1.86, suggesting that the graphene film is of multilayer with few defects.[25] With regard to the spectrum of Ga_2O_3, there are several representative peaks at 201, 348, 417 and 653 cm^{-1}, attributable to the Raman shift of beta-Ga_2O_3.[26] Electrical analysis in Figure 1f reveals that the MLG-Ga_2O_3 heterojunction displays a typical asymmetrical metal-semiconductor-metal transport property. Considering the good contact between the MLG and silver (Figure S2, Supporting Information), the above nonlinear *I*–*V* characteristics can be ascribed to two back-to-back Schottky barriers, one is formed at Cr/Au-Ga_2O_3 contact and the other one is formed at Ga_2O_3-MLG contact (inset of Figure 1f).

When the MLG-Ga_2O_3 heterojunction was shined with 365 nm light, the *I*–*V* curve is virtually identical to that in dark (**Figure 2**a), suggesting that MLG-Ga_2O_3 device is blind to 365 nm illumination. However, it is interesting to note that further illumination of UV light with wavelength of 254 nm will lead to a considerable increase in current at forward bias voltage, as shown in Figure 2b. This enhancement in photocurrent leads to the well-defined rectifying characteristics of MLG-Ga_2O_3, that is, the carriers can only flow in one way

W.-Y. Kong, G.-A. Wu, K.-Y. Wang, T.-F. Zhang, Y.-F. Zou, D.-D. Wang, Prof. L.-B. Luo
School of Electronic Science and Applied Physics
Hefei University of Technology
Hefei, Anhui 230009, P. R. China
E-mail: luolb@hfut.edu.cn

DOI: 10.1002/adma.201604049

© 2016 WILEY-VCH Verlag GmbH & Co. KGaA, Weinheim

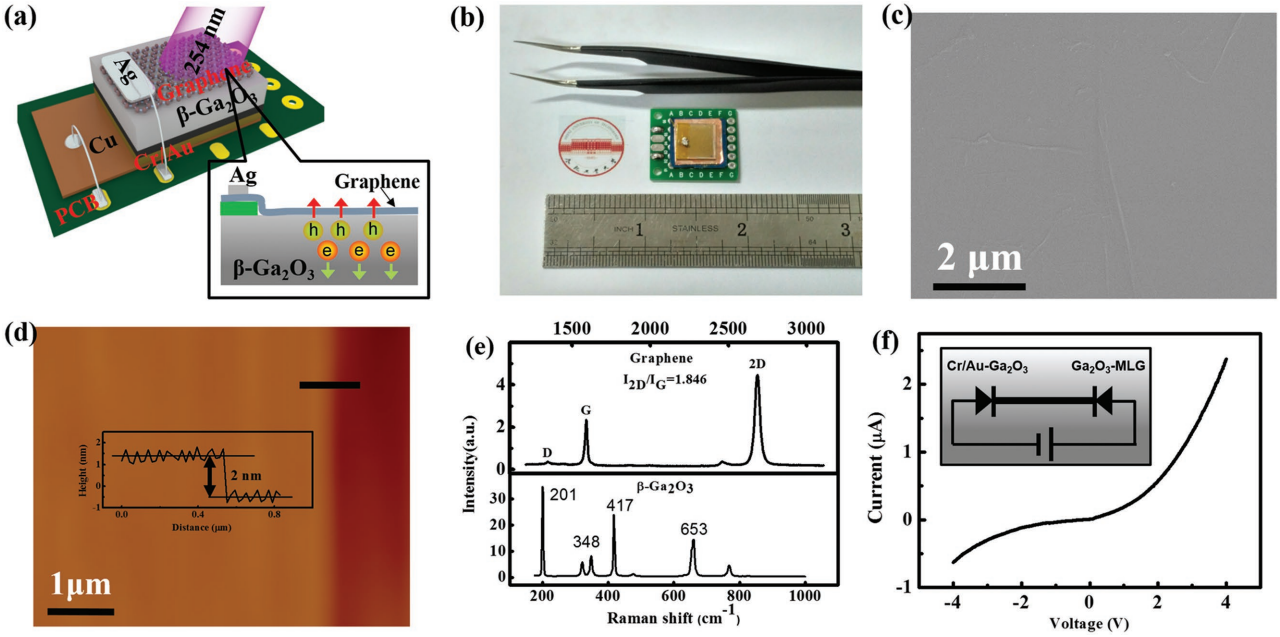

Figure 1. a) Schematic diagram of the MLG/β-Ga_2O_3 wafer DUVPD. b) A digital photograph of the device. c) FESEM image of MLG on the surface of a β-Ga_2O_3 wafer. d) AFM image of a typical MLG film on Ga_2O_3 wafer. e) Raman spectrum of the MLG film and β-Ga_2O_3 wafer. f) *I–V* characteristics of the DUVPD measured at room temperature in dark, the inset shows the device model of two back-to-back Schottky diodes.

fashion. Understandably, this sensitivity to DUV illumination can be exclusively attributed to the contribution from MLG-Ga_2O_3 given that the incident DUV is as weak as e^{-2762} of its initial intensity when it reaches the Cr/Au-Ga_2O_3 interface (please refer to the detailed calculation in the Supporting Information). To explore the stability of this photoelectric effect due to MLG-Ga_2O_3, the UV illumination of 254 nm light was alternately turned on and off. Figure 2c shows the photoresponse of the device at a bias voltage of 4 V, from which it can be seen that the MLG-Ga_2O_3 heterojunction device can be readily switched between "on" and "off" states for 50 cycles. By deducing one cycle of the photoresponse of the DUVPD (Figure S3, Supporting Information), both rise and fall time were estimated to be 94.83 and 219.19 s, respectively, which are relatively slower than other Ga_2O_3 structures based devices. As a matter of fact, the present device can keep nearly the identical photocurrent and work properly even after one month storage at ambient condition. Such excellent stability and reproducibility is understandably owing to both graphene film and Ga_2O_3 wafer, which are highly stable in air. Figure 2d plots the current of the MLG-Ga_2O_3 heterojunction under DUV illumination at different bias voltages in the range from 2 to 8 V. It is clear from the Figure 2e that the photocurrent will increase monotonically with increasing bias voltage. This evolution is related to increased drift velocity of photogenerated charge carriers and suppressed recombination possibility at high bias voltage.[27,28]

In addition to the bias voltage, the photoresponse is dependent on the light intensity as well. **Figure 3**a shows the *I–V* curves under UV light illumination with intensity ranging from 57 to 488 μW cm^{-2}. Apparently, under different intensities, the as-assembled MLG-Ga_2O_3 heterojunction device always exhibit typical rectifying characteristics. In addition, the photocurrent was observed to increase with increasing light intensity at forward bias voltage. Further photoresponse characteristic in Figure 3b shows that the MLG-Ga_2O_3 device can be switched between on and off states under varied light intensities with good reproducibility. Figure 3c plots the quantitative relationship between the photocurrent versus incident light intensities which are extracted from Figure 3b at a bias voltage of 4 V. The photocurrent exhibits a power-law dependence on the light intensity with an exponent of 0.73 ($I_p = P^{0.73}$). This noninteger exponent is associated with the trap states due to defect species from either MLG layer or Ga_2O_3 wafer.[29,30]

To quantitatively assess the device performance of the present DUVPD, both responsivity (R) and detectivity (D^*) were calculated. The responsivity which is defined as the photocurrent generated per unit power of the incident light on the effective area of a photodetector can be estimated using the following equation

$$R = \frac{I_\lambda - I_d}{P_\lambda S} \tag{1}$$

where I_λ is the photocurrent, P_λ is the light intensity, I_d is the dark current, S is the effective illuminated area (S = 0.8 cm^2). By using the above equation, and many experimental values ($I_\lambda = 3.75 \times 10^{-4}$ A, $I_d = 1.1 \times 10^{-6}$ A, $P_\lambda = 3.15 \times 10^{-4}$ W cm^{-2}), the R_λ at a bias voltage of 2 V was estimated to be 1.48 A W^{-1}.

The detectivity that is usually used to describe the smallest detectable signal, can be described by the following equation

$$D^* = \frac{R_\lambda A^{1/2}}{(2eI_d)^{1/2}} \tag{2}$$

where R_λ is the responsivity, A is the effective area of the DUVPD channel (A = 0.8 cm^2), e is the electronic charge,

© 2016 WILEY-VCH Verlag GmbH & Co. KGaA, Weinheim

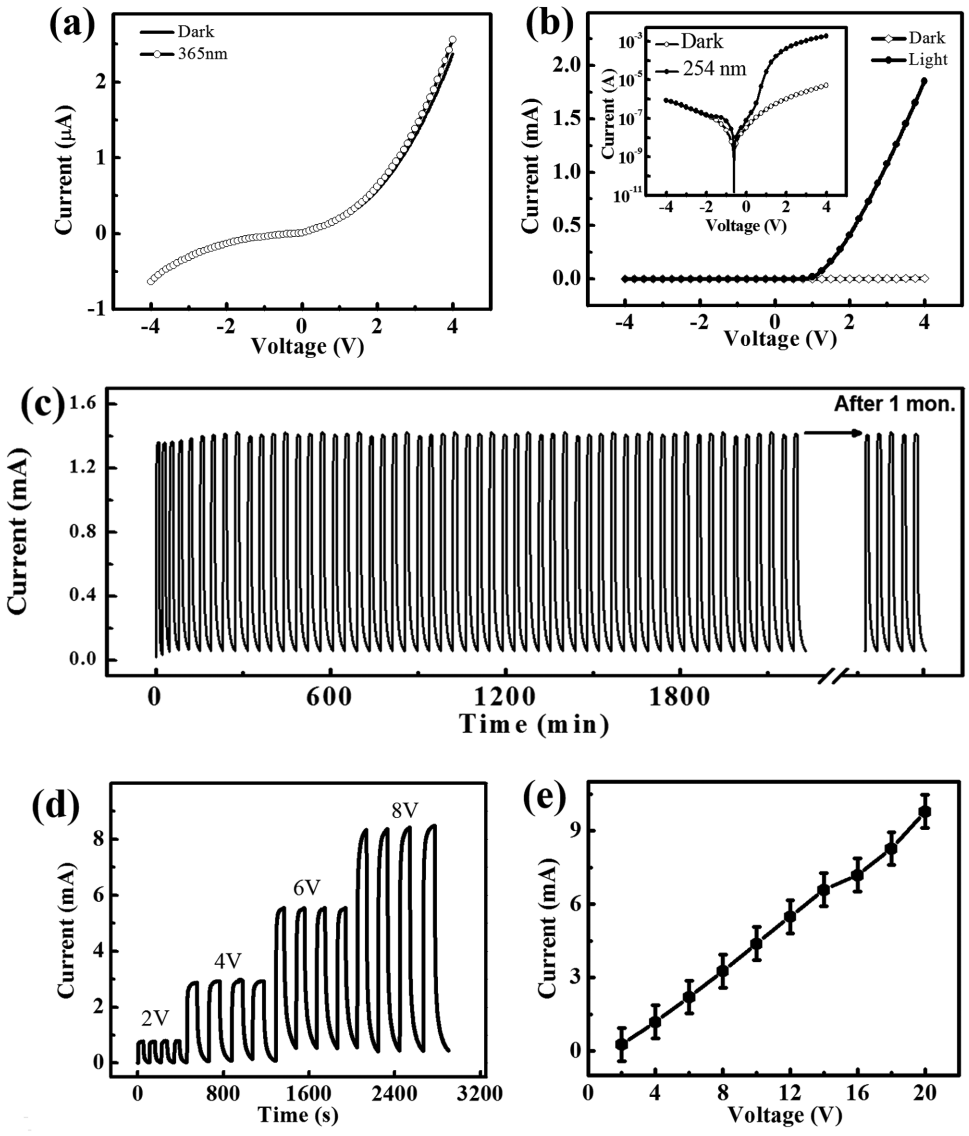

Figure 2. a) *I–V* characteristics of the MLG-Ga_2O_3 heterojunction DUVPD in dark and under 365 nm light irradiation. b) *I–V* characteristics of the device in dark and under 254 nm light irradiation, the inset shows the *I–V* curves on a logarithmic scale. c) Photoresponse of the DUVPD for 55 cycles, the last five cycles correspond to the photoresponse after storage for one month. d) Current of the DUVPD under UV light illumination at bias voltages of 2, 4, 6, and 8 V. e) Photocurrent as a function of the bias voltage.

and I_d is the dark current. Based on the Equation (2) as well as many constants derived from experiment (R_λ = 1.48 A W^{-1}, $I_d = 1.1 \times 10^{-6}$ A, $e = 1.602 \times 10^{-19}$ C), the D^* at a bias voltage of 2 V was calculated to be 2.24×10^{12} Jones. **Figure 4**a plots both R and D^* at various bias voltages. It is obvious that in the voltage from 2–20 V, both parameters increase considerably with increasing bias voltage. Specifically, the responsivity and detectivity are as high as 39.3 A W^{-1} and 5.92×10^{13} Jones at 20 V, respectively. As a matter of fact, similar evolution was also observed on external quantum efficiency (EQE), which is defined as the number of electrons probed per incident photon and can be estimated by the equation: EQE = $hcR_\lambda/(e\lambda)$, where I_λ is the photocurrent, P_λ is the light intensity, S is the effective illuminated area of DUVPD (S = 0.8 cm^2), h is the Planck's constant, c is the velocity of light, e is the electronic charge, and λ is the exciting wavelength of DUV, respectively. As shown in Figure 4b, the EQE at a bias voltage of 2 V was 7.27×10^2%. It gradually increases with increasing bias voltage and is as high as 1.98×10^4% when the bias voltage reaches 20 V. Such a relationship according to previous study is reasonable as high bias voltage can cause increased probability of exciton separation and acceleration, and enhanced electric field, which will facilitate the photogeneration of more carriers, leading to higher photocurrent in the circuit.[31] Besides bias voltage, the responsivity, detectivity, and EQE are all dependent on the DUV light intensity as well. Figure 4c,d shows the responsivity, detectivity, and EQE under illumination of various DUV light intensities. It is clear that all the three metrics were found to decrease with increasing light intensity. This finding is probably due to the self-heating at high light intensity, which will induce

© 2016 WILEY-VCH Verlag GmbH & Co. KGaA, Weinheim

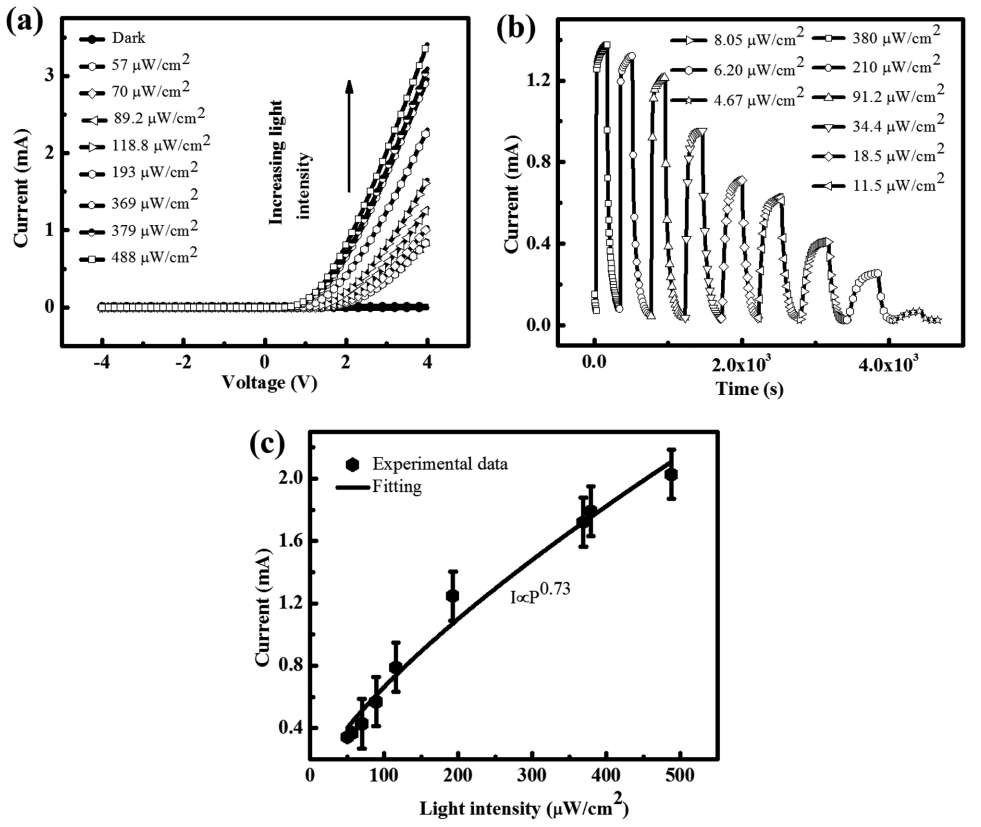

Figure 3. a) The current–voltage curves of the MLG-Ga_2O_3 heterojunction DUVPD under 254 nm light with different intensities. b) Photoresponse of the device under different light intensities. c) The relationship between the light intensity and photocurrent.

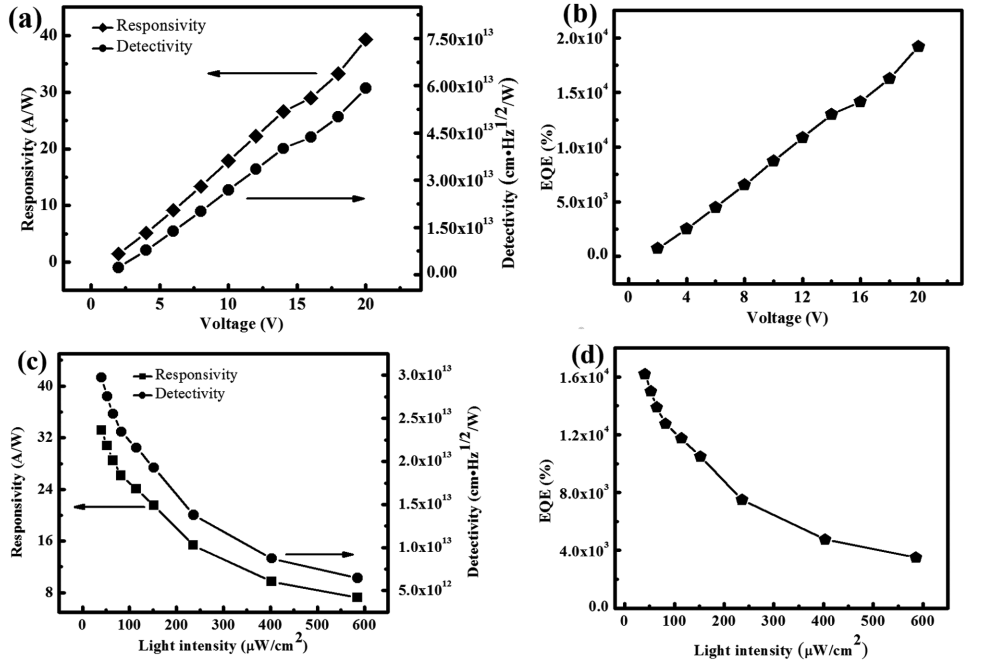

Figure 4. a) Both responsivity and detectivity of the MLG-Ga_2O_3 heterojunction DUVPD at different bias voltages. b) The EQE as a function of bias voltage. c) Both responsivity and detectivity the MLG-Ga_2O_3 heterojunction DUVPD under light illumination with different intensities. d) The EQE as a function of light intensity.

© 2016 WILEY-VCH Verlag GmbH & Co. KGaA, Weinheim

Table 1. Comparison of the device parameters of the present MLG-Ga_2O_3 heterojunction DUVPD and other Ga_2O_3 nanostructures based devices.

Materials and structures	R [A W^{-1}]	D^* [cmHz$^{1/2}$ W^{-1}]	G	EQE [%]	Reference
Graphene/β-Ga_2O_3 wafer	39.3	5.92×10^{13}	192.5	1.96×10^4	Our work
ZnO-Ga_2O_3 core–shell heterojunction	5.18×10^3	9.9×10^{14}	–	2.53×10^6	[33]
2-D β-Ga_2O_3 nanosheet	3.3	4.0×10^{12}	–	1600	[34]
Ga_2O_3 nanobelt	37.6	–	–	1.87×10^2	[35]
Ga_2O_3 nanowire	3.43×10^{-3}	–	–	1.37	[36]
IZO/β-Ga_2O_3/IZO M-S-M structure	3.2×10^{-4}	2.8×10^{10}	≈1	0.2	[37]
Ga_2O_3/SnO_2:Ga core–shell nanowire	2.54×10^{-2}	–	–	0.362	[38]

not only increased charge carrier scattering but also increased recombination possibility.[32] **Table 1** lists several important device metrics of a couple of photodetectors that were made of other Ga_2O_3 nanostructures with various device geometries. It can be seen that the device performance including responsivity, detectivity and EQE are poorer than that the device composed of ZnO-Ga_2O_3 core–shell micro-heterojunction.[33] However, these key parameters are not only better than the devices based on 2-D β-Ga_2O_3 nanosheet,[34] Ga_2O_3 nanobelt,[35] and β-Ga_2O_3 nanowire[36] but also those made of indium zinc oxide (IZO)/β-Ga_2O_3/IZO (M-S-M structure),[37] and Ga_2O_3/SnO_2:Ga core–shell.[38] Such relatively high performance, along with the easy construction and low fabrication cost renders the present simply structured DUVPD promising building blocks for high-performance optoelectronic system in the future.

In order to evaluate the selectivity of the present MLG-Ga_2O_3 DUVPD, the spectral response in the range from 200–800 nm was measured and shown in **Figure 5**. It can be seen that the heterojunction device displays an excellent wavelength selectivity: It is highly sensitive to photons with wavelength less than 220 nm, but when the wavelength is longer than 220 nm, the sensitivity decreases gradually and reaches a minimum value at about 280 nm. Further illumination of photons with wavelength larger than 280 nm can hardly induce obvious photocurrent. Such spectral selectivity with peak sensitivity at ≈220 nm corresponds to the intrinsic absorption of Ga_2O_3 wafer. Understandably, this consistence is believed to be due to the working mechanism of MLG-Ga_2O_3 heterojunction DUVPD. The photosensitivity of the MLG-Ga_2O_3 heterojunction solar-blind DUVPD can be interpreted by the energy band diagram at forward bias voltage shown in Figure 5b. When MLG was coated on the Ga_2O_3 wafer, the electrons in the latter move to the MLG, and as a result, the energy levels near the *n*-type Ga_2O_3 bend upward, causing the formation of built-in electric field near the MLG-Ga_2O_3 contact (the depletion region). Once irradiated by UV lights with wavelength less than 254 nm (the bandgap of Ga_2O_3 is 4.9 eV, corresponding to 254 nm), the Ga_2O_3 will absorb the photons and lift the electrons in the valence band to conduction band, leading to formation of photo-excited electron–hole pairs. Thanks to the presence of electric field, the photogenerated electron–hole pairs in the depletion region will be separated and then move toward opposite directions (the holes moves toward MLG, while the electrons move toward Ga_2O_3), forming the photocurrent in the circuit. Such a photoelectric process happens only on condition that the energy incident UV light is larger than the bandgap of the Ga_2O_3.

To validate the carrier collection capability of the MLG during the above photoelectric process, we then investigated the photocurrent mapping profile of the DUVPD by moving the DUV illumination at selected grid (as shown in Figure S4a,b in the Supporting Information, there are totally 25 grids). Figure S4c (Supporting Information) displays the spatially resolved photocurrent mapping profile which was obtained by moving the light illumination from one grid to another. The measured

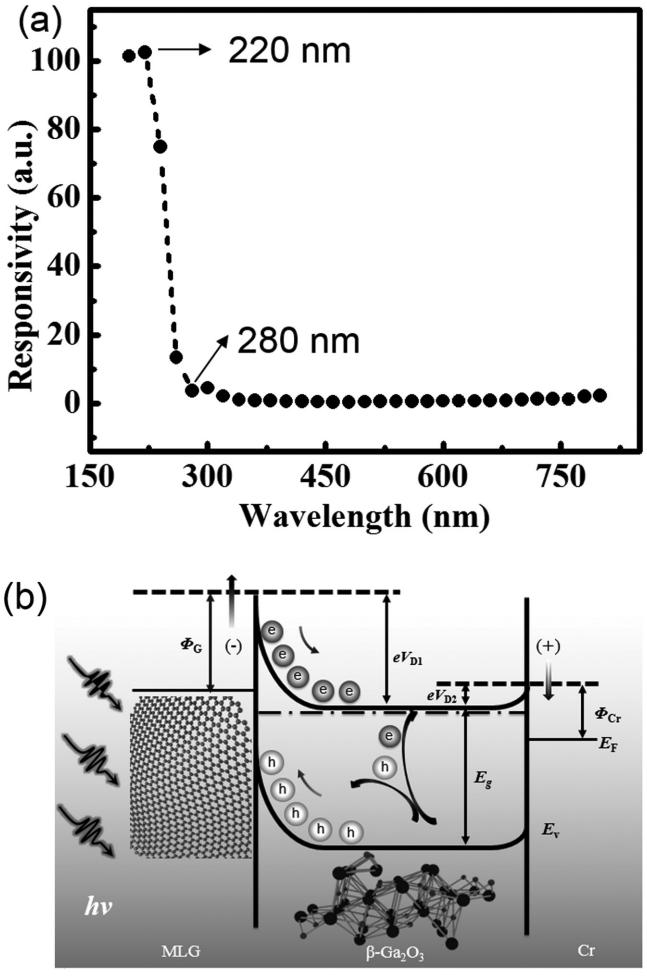

Figure 5. a) Normalized spectral selectivity of the MLG-Ga_2O_3 heterojunction DUVPD. b) Energy band diagram of the MLG-Ga_2O_3 heterojunction DUVPD at forward bias voltage.

© 2016 WILEY-VCH Verlag GmbH & Co. KGaA, Weinheim

photocurrent corresponding to each grid was demonstrated by a 2D plot to show the contrast maps. It is clear that photocurrent ranges from 1.0–1.68 × 10^{-5} A, with a relatively narrow distribution which is probably related to the poor contact at the wrinkles, as observed in Figure 1c. This relatively uniform photocurrent distribution suggests that the present MLG-Ga_2O_3 DUVPD can be further miniatured to achieve integrated optoelectronic system for DUV image sensing.

In this study, we report a simple DUVPD which was fabricated by directly transferring a layer of MLG film on *n*-type Ga_2O_3 wafer. Electrical analysis revealed that the MLG-Ga_2O_3 heterojunction device displays pronounced rectifying characteristic under DUV light illumination. It was also revealed that DUVPD was highly sensitive to 254 nm UV light illumination with very good stability and reproducibility. The corresponding device parameters including responsivity and detectivity were comparable to or even better than other low-dimensional Ga_2O_3 nanostructures based photodetectors. Further device analysis found that the DUVPD was highly sensitive to UV light with wavelength less than 254 nm, but was nearly blind to photons with wavelength longer than 280 nm. These results signify that the present simply structured MLG-Ga_2O_3 DUVPD may find potential applications in future optoelectronic devices.

Experimental section

Materials Synthesis and Device Fabrication: The *n*-type mono-crystalline Ga_2O_3 wafer (size: 10 × 10 × 0.6 mm^3) was purchased from the Hefei Kejing Mater. Tech. Co. Ltd. The substrate was doped with Sn atoms with a carrier concentration of 2–9 × 10^{18} cm^2 V^{-1} s^{-1}. The graphene film used in this work was synthesized by a conventional chemical vapor deposition method, which used 50 µm Cu foils as catalytic substrate and a mixed of CH_4 and H_2 as precursor.[39] To assemble the graphene-Ga_2O_3 heterojunction device, an *n*-type Ga_2O_3 wafer was first cleaned with alcohol and acetone under ultrasonication for 10 min, and then covered with a layer graphene film supported by polymethyl methacrylate (the detailed information about synthesis and transfer of MLG can be found elsewhere[15]). Afterward, silver paste was stuck at the periphery of the Ga_2O_3 wafer. The as-assembled device was then transferred onto a PCB for device analysis.

Material Characterization and Device Analysis: The MLG film was studied by a Raman spectrometer (Horiba Jobin Yvon, LabRAM HR800), The optoelectronic property of the MLG-Ga_2O_3 Schottky junction DUVPD was investigated by an *I–V* semiconductor characterization system (4200-SCS, Keithley Co. Ltd) equipped with a monochromatic (SP2150, Princeton Co.) from which the incident UV light was directly focused and guided onto the device. The 254 and 365 nm lasers were bought from Tanon Sci. Tech. Com. (Tanon, UV-100). Prior to device analysis, the power intensity of the incident light was calibrated by a powermeter (Thorlabs GmbH., PM 100D).

Supporting Information

Supporting Information is available from the Wiley Online Library or from the author.

Acknowledgements

This work was supported by the Natural Science Foundation of China (NSFC, Grant Nos. 61575059 and 61675062) and the Fundamental Research Funds for the Central Universities (Grant Nos. 2012HGCX0003, 2013HGCH0012, and 2014HGCH0005).

Received: July 29, 2016
Revised: August 30, 2016
Published online: October 17, 2016

[1] S. Assefa, F. N. Xia, Y. A. Vlasov, *Nature* **2010**, *464*, 80.
[2] L. Peng, L. F. Hu, X. S. Fang, *Adv. Mater.* **2013**, *25*, 5321.
[3] B. Nie, J. G. Hu, L. B. Luo, C. Xie, L. H. Zeng, P. Lv, F. Z. Li, J. S. Jie, M. Feng, C. Y. Wu, Y. Q. Yu, S. H. Yu, *Small* **2013**, *9*, 2872.
[4] K. K. Manga, S. Wang, M. Jaiswal, Q. L. Bao, K. P. Loh, *Adv. Mater.* **2010**, *22*, 5265.
[5] Y. B. Li, T. Tokizona, M. Y. Liao, M. Zhong, Y. Koide, I. Yamada, J. J. Delaunay, *Adv. Funct. Mater.* **2010**, *20*, 3972.
[6] R. J. Zou, Z. Y. Zhang, Q. Liu, J. Q. Hu, L. W. Sang, M. Y. Liao, W. J. Zhang, *Small* **2014**, *10*, 1848.
[7] L. Li, E. Auer, M. Y. Liao, X. S. Fang, T. Y. Zhai, U. K. Gautam, A. Lugstein, Y. Koide, Y. Bando, D. Golberg, *Nanoscale* **2011**, *3*, 1120.
[8] W. Tian, C. Y. Zhi, T. Y. Zhai, S. M. Chen, X. Wang, M. Y. Liao, D. Golberg, Y. Bando, *J. Mater. Chem.* **2012**, *22*, 17984.
[9] W. Feng, X. N. Wang, J. Zhang, L. F. Wang, W. Zheng, P. A. Hu, W. W. Cao, B. Yang, *J. Mater. Chem.* **2014**, *2*, 3254.
[10] S. F. Leung, Q. P. Zhang, F. Xiu, D. L. Yu, J. C. Ho, D. D. Li, Z. Y. Fan, *J. Phys. Chem. Lett.* **2014**, *5*, 1479.
[11] W. Y. Weng, T. J. Hsueh, S. J. Chang, G. J. Huang, H. T. Hsueh, *IEEE Photonics Tech. Lett.* **2011**, *23*, 444.
[12] C. L. Hsu, Y. C. Lau, *Nanoscale* **2012**, *4*, 5710.
[13] B. Zhao, F. Wang, H. Y. Chen, Y. P. Wang, M. Jiang, X. S. Fang, D. X. Zhao, *Nano Lett.* **2015**, *15*, 3988.
[14] S. J. Kim, T. H. Seo, M. J. Kim, K. M. Song, E. K. Suh, H. S. Kim, *Nano Res.* **2015**, *8*, 1327.
[15] P. Wang, X. Q. Li, Z. J. Xu, Z. Q. Wu, S. J. Zhang, W. L. Xu, H. K. Zhong, H. S. Chen, E. P. Li, J. K. Luo, Q. K. Yu, S. S. Lin, *Nano Energy* **2015**, *13*, 509.
[16] R. J. Shiue, Y. D. Gao, Y. F. Wang, C. Peng, A. D. Bobertson, D. K. Efetov, S. Assefa, F. H. L. Koppens, J. Hone, D. Englud, *Nano Lett.* **2015**, *3*, 4723.
[17] L. H. Zeng, M. Z. Wang, H. Hu, B. Nie, Y. Q. Yu, C. Y. Wu, L. Wang, J. G. Hu, C. Xie, F. X. Liang, L. B. Luo, *ACS Appl. Mater. Interfaces* **2013**, *5*, 9362.
[18] X. M. Li, H. W. Zhu, K. L. Wang, A. Y. Cao, J. Q. Wei, C. Y. Li, Y. Jia, X. Li, D. H. Wu, *Adv. Mater.* **2010**, *22*, 2743.
[19] Y. Song, X. M. Li, C. Mackin, X. Zhang, W. J. Fang, T. Palacios, H. W. Zhu, J. Kong, *Nano Lett.* **2015**, *15*, 2104.
[20] X. H. An, F. Z. Liu, Y. J. Jung, S. Kar, *Nano Lett.* **2013**, *13*, 909.
[21] T. Dufux, J. Boettcher, M. Burghard, K. Kern, *Small* **2010**, *6*, 1867.
[22] Y. Kim, S. J. Kim, S. P. Cho, B. H. Hong, D. J. Jang, *Sci. Rep.* **2015**, *5*, 12345.
[23] A. K. Geim, K. S. Novoselov, *Nat. Mater.* **2007**, *6*, 183.
[24] K. S. Novoselov, A. K. Geim, S. V. Norozov, D. Jiang, M. I. Katsnelson, I. V. Grigorieva, S. V. Dubonos, A. A. Firsov, *Nature* **2005**, *438*, 197.
[25] N. G. Shang, P. Papakonstantinou, M. Mc Mullan, M. Chu, A. Stamboulis, A. Potenza, S. S. Dhesi, H. Marchetto, *Adv. Funct. Mater.* **2008**, *18*, 3506.
[26] S. Kumar, R. Singh, *Phys. Status Solidi* **2013**, *10*, 781.

© 2016 WILEY-VCH Verlag GmbH & Co. KGaA, Weinheim

[27] C. Soci, A. Zhang, B. Xiang, S. A. Dayes, D. P. R. Aplin, J. Park, X. Y. Bao, Y. H. Lo, D. Wang, *Nano Lett.* **2007**, *7*, 1003.
[28] J. G. Ok, J. Y. Lee, H. W. Baac, S. H. Tawfick, L. J. Guo, A. J. Hart, *ACS Appl. Mater. Interfaces* **2014**, *6*, 874.
[29] N. V. Joshi, *Photoconductivity: Art, Science, and Technology*, Marcel Dekker, New York **1990**.
[30] H. Kind, H. Yan, B. Messer, M. Law, P. Yang, *Adv. Mater.* **2002**, *14*, 158.
[31] L. Liu, Z. S. Su, Q. Y. Xi, G. Gao, W. Yang, Y. X. Zhao, C. Q. Wu, L. D. Wang, J. W. Xu, *Appl. Phys. Lett.* **2016**, *108*, 163504.
[32] B. D. Boruah, A. Mukherjee, A. Misra, *Nanotechnology* **2016**, *27*, 095205.
[33] B. Zhao, F. Wang, H. Y. Chen, Y. P. Wang, M. M. Jiang, X. S. Fang, D. X. Zhao, *Nano. Lett.* **2015**, *15*, 3988.
[34] W. Feng, X. N. Wang, J. Zhang, L. F. Wang, W. Zheng, P. A. Hu, W. W. Cao, B. Yang, *J. Mater. Chem. C* **2014**, *2*, 3254.
[35] L. Li, E. Auer, M. Y. Liao, X. S. Fang, T. Y. Zhai, U. K. Gautam, A. Lugstein, Y. Koide, Y. Bando, D. Golberg, *Nanoscale* **2011**, *3*, 1120.
[36] Y. L. Wu, S. J. Chang, W. Y. Weng, C. H. Liu, T. Y. Tsai, C. L. Hsu, K. C. Chen, *IEEE Sens. J.* **2013**, *6*, 2368.
[37] T. C. Wei, D. S. Tsai, P. Ravadgar, J. J. Ke, M. L. Tsai, D. H. Lien, C. Y. Huang, R. H. Horng, J. H. He, *IEEE J. Sel. Top Quantum Electron* **2014**, *20*, 3802006.
[38] C. L. Hsu, Y. C. Lu, *Nanoscale* **2012**, *4*, 5710.
[39] X. Z. Zhang, C. Xie, J. S. Jie, X. W. Zhang, Y. M. Wu, W. J. Zhang, *J. Mater. Chem. A* **2013**, *1*, 6593.

© 2016 WILEY-VCH Verlag GmbH & Co. KGaA, Weinheim